Influence of the arc plasma parameters on the weld pool profile in TIG welding

To cite this article: A Toropchin *et al* 2014 *J. Phys.: Conf. Ser.* **550** 012004

Journal of Physics: Conference Series **550** (2014) 012004 doi:10.1088/1742-6596/550/1/012004

Influence of the arc plasma parameters on the weld pool profile in TIG welding

A Toropchin[1], V Frolov[1], A V Pipa[2], R Kozakov[2], and D Uhrlandt[2]

[1]Saint Petersburg State Polytechnical University, 29 Polytechnicheskaya, 195251 Saint-Petersburg, Russia,

[2] Leibniz Institute for Plasma Science and Technology (INP Greifswald), Felix-Hausdorff-Str. 2, 17498 Greifswald, Germany

E-mail: frolov.eed@gmail.com

Abstract. Magneto-hydrodynamic simulations of the arc and fluid simulations of the weld pool can be beneficial in the analysis and further development of arc welding processes and welding machines. However, the appropriate coupling of arc and weld pool simulations needs further improvement. The tungsten inert gas (TIG) welding process is investigated by simulations including the weld pool. Experiments with optical diagnostics are used for the validation. A coupled computational model of the arc and the weld pool is developed using the software ANSYS CFX. The weld pool model considers the forces acting on the motion of the melt inside and on the surface of the pool, such as Marangoni, drag, electromagnetic forces and buoyancy. The experimental work includes analysis of cross-sections of the workpieces, high-speed video images and spectroscopic measurements. Experiments and calculations have been performed for various currents, distances between electrode and workpiece and nozzle diameters. The studies show the significant impact of material properties like surface tension dependence on temperature as well as of the arc structure on the weld pool behaviour and finally the weld seam depth. The experimental weld pool profiles and plasma temperatures are in good agreement with computational results.

1. Introduction

Tungsten Inert Gas (TIG) welding was developed in 1940s, and since the beginning it is widely applied in industry and a continuously improved technology. It is based on the process of the heat transfer by the electric arc from the non-consumable tungsten cathode to the workpiece-anode. Straight polarity is suitable for steels, investigated in the present article, to maximize the welding penetration and minimize the cathode heating. For aluminium, for example, the alternating current is more suitable for surface oxide layer damaging in the reverse polarity period and tungsten cathode cooling with maximum workpiece heating in the straight polarity period. The reverse polarity is never used to avoid melting of the tungsten electrode and the consequent contamination of the weld pool.

The process of TIG welding is operated with arc and weld pool shielding by an inert gas. As inert gas welders use argon or helium. Choice of the inert gas is based on the industrial requirements and purposes. The helium arc produces deeper penetration, but helium is more expensive than argon. That is the reason for applications of argon and helium mixtures. One of the advantages of TIG welding is that addition of filler in the weld pool is optional. Use of

filler rods is mandatory in particular for thick workpieces (above 34 mm) to make a seam with required quality and mechanical characteristics.

The TIG process is typically ignited by a high-voltage and high-frequency oscillator to avoid contamination of the weld pool by molten tungsten. In contrast, other types of welding processes, gas metal arc welding (GMAW) for example, can be ignited simply with the touch of the two electrodes.

TIG welding processes use arc plasmas with maximum temperatures in the range from 12000 to 20000 K depending on current and voltage. These values are high enough to melt the metal and weld two metal pieces.

The present article is focused on the classic TIG welding, but also investigates and compares the results considering a setup similar to plasma welding. Therefore, the tungsten cathode is placed inside a narrow ceramic nozzle. However, the second nozzle typically used in plasma welding was not applied in the present study. Plasma welding processes are characterized by a compressed arc with elevated temperatures. The compression also increases the depth of weld penetration and decreases the heat-affected zone. Mechanical characteristics of the seams welded by plasma welding can be improved in comparison with classic TIG welding.

Welding as other fields of industry is on the way of continuous progress. Adding new materials in the cathode material, like lanthanum or thorium, to increase it heat resistance, new nozzles with improved inert gas flow etc are one side of the progress. The goal of welding process modeling is to minimize the experimental part for improving the construction of plasma torches or other process improvements in industry or in laboratories. The models must be reliable and include a large number of physical processes to consider the forces acting on the arc, on the motion of the melt inside and on the surface of the pool. The present investigation is focussed on the examination of one of these forces, the necessity to consider the Marangoni force acting on the weld pool profile. Marangoni force, its mathematical formulation and its influence on the shape of the weld pool, depending on the value of the surface tension of the metal have been considered in several papers [1, 2, 3]. Present article describes a method of surface tension calculation of steel depending on the temperature of the metal. Also the investigations of various welding modes, such as arc current and arc length, and various nozzles tip have been done to estimate the efficiency of process and accuracy of simulation model.

2. Simulation model

The time dependent two-dimensional coupled computational model of the arc and the weld pool was developed using software ANSYS CFX. The main governing equations include mass continuity (1), momentum conservation (2),(3), energy conservation (4):

$$\frac{\partial}{\partial z}\left(\rho V_z\right)+\frac{1}{r}\frac{\partial}{\partial r}\left(r\rho V_r\right)=0 \tag{1}$$

$$\rho\left(V_z\frac{\partial V_r}{\partial z}+V_r\frac{\partial V_r}{\partial r}\right)=-\frac{\partial p}{\partial r}+\left[\vec{J}\times\vec{B}\right]_r+\frac{\partial}{\partial z}\left(\mu\frac{\partial V_r}{\partial z}\right)+\frac{1}{r}\frac{\partial}{\partial r}\left(r\mu\frac{\partial V_r}{\partial r}\right)-\mu\frac{V_r}{r^2} \tag{2}$$

$$\rho\left(V_z\frac{\partial V_r}{\partial z}+V_r\frac{\partial V_r}{\partial r}\right)=-\frac{\partial p}{\partial z}+\left[\vec{J}\times\vec{B}\right]_z+\frac{\partial}{\partial z}\left(\mu\frac{\partial V_z}{\partial z}\right)+\frac{1}{r}\frac{\partial}{\partial r}\left(r\mu\frac{\partial V_z}{\partial r}\right)+\rho g_z \tag{3}$$

$$\rho V_z\frac{\partial H}{\partial z}+\frac{1}{r}\rho V_r\frac{\partial H}{\partial r}=\sigma E^2-U_{\mathrm{rad}}+\frac{\partial}{\partial z}\left(\frac{\lambda}{C_{\mathrm{p}}}\frac{\partial H}{\partial z}\right)+\frac{1}{r}\frac{\partial}{\partial r}\left(r\frac{\lambda}{C_{\mathrm{p}}}\frac{\partial H}{\partial r}\right), \tag{4}$$

where ρ is mass density, V_z and V_r are axial and radial velocity components, p is pressure, $\vec{J}$ is electric current density, $\vec{B}$ is magnetic field, μ is viscosity, g_z is gravitational acceleration, H is enthalpy, σ is electrical conductivity, E is electric field strength, U_{rad} is energy losses due to radiation, λ is thermal conductivity and C_{p} is heat capacity at constant pressure. Along with these the current continuity coupled with Ohms law and Maxwells equations similar to those

in [1] are used. The boundary conditions were set according to experimental values to meet gas flow rate, electric current and ambient temeprature.

Also, the forces acting on the weld pool, such as drag force by the arc, buoyancy, electromagnetic force and Marangoni force are included in the model [1, 2, 3]. Such effects as metal vapour, turbulence of plasma flow and the movement of the weld pool surface are neglected due to its lower impact on the main behavior of the TIG arc under the conditions considered in this work. The radiative, thermodynamic and transport properties are taken from [4, 5]. The inhomogeneous mesh is used to run the simulations faster. The mesh is different for various geometric configurations and has 30000 cells in average. The smallest cell is 0.03 mm x 0.1 mm in the domain of arc burning and workpiece melting, the biggest one 0.2mm x 2mm in the domain of gas outflow. The most important force affecting the profile of the weld pool is the Marangoni force, which is the phenomenon of mass transfer along the interface between two fluids that occurs due to the presence of the gradient of the surface tension. The higher the surface tension of the liquid, the higher force tighten the surface. Therefore, the liquid moves to the domain with the greater coefficient of surface tension [10]. The Marangoni force is given by

$$M_A = \frac{\partial}{\partial z}\left(\frac{\partial \gamma}{\partial T}\frac{\partial T}{\partial r}\right) \tag{5}$$

where γ is the surface tension of the molten pool and T the workpiece temperature [1]. The influence of the Marangoni force is best illustrated by the following example: comparing a material with falling surface tension characteristic and a material like mild steel with rising characteristic. The dependence of weld pool profile and direction of molten metal movement on the surface tension is shown in figure 1 [2].

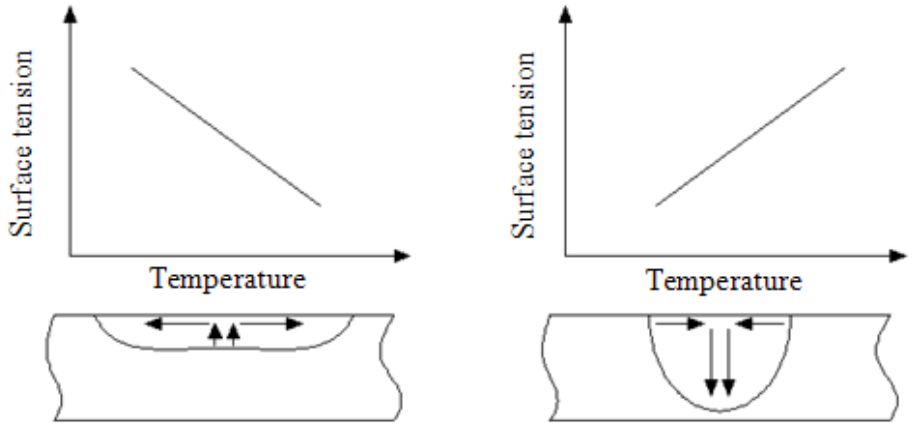

Figure 1. Schematic illustration of convection in the weld pool driven by Marangoni force resulting from the temperature dependence of the surface tension.

As the workpiece material in the present study steel S235 with following composition is considered: C=0.17%, Mn=1.4%, P=0.035%, S=0.035%, N=0.012%, Fe=97.8%. The surface tension of steel S235 in liquid condition is required. Using the reference data [11, 12], the parameters of capillary activity F_{1873} were obtained for the temperature 1873 K.

From the values of capillary activity, atomic weight and percentage content of the elements presented in table 1 the surface tension of the alloy was calculated using the following equation [11]

Table 1. Element data of steel S235

Element	C	Mn	P	S	N	Fe
F_{1873}	2.0	5.0	1.5	500.0	150.0	1
Atomic weight	12	55	31	32	24	56
Number of moles, n_i	0.0140	0.0260	0.0010	0.0010	0.0009	1.746
$\sum n_i$			1.807			
Atomic part in steel, $X_i = \frac{n_i}{\sum n_i}$	0.0080	0.0140	0.0006	0.0006	0.0005	0.966
$X_i \cdot F_{1873}$	0.016	0.070	0.001	0.275	0.072	0.966
$\sum X_i \cdot F_{1873}$			1.4			

$$\gamma = \gamma_{\mathrm{Fe}} - 2000 \log \left(\sum X_i F_T \right) \tag{6}$$

where γ_{Fe} is the surface tension of pure iron for the respective temperature. Thus, the surface tension value for steel S235 at 1873 K is $\gamma_{1873} = 1.551$ N/m. The capillary activity and the surface tension were calculated for other temperatures using the following equation [11].

$$F_T = F_{1873}^{\frac{1873}{T}} \tag{7}$$

The surface tension of steel S235 as a function of temperature is shown in figure 2. It decreases down to 1.431 N/m at 2300 K, for example.

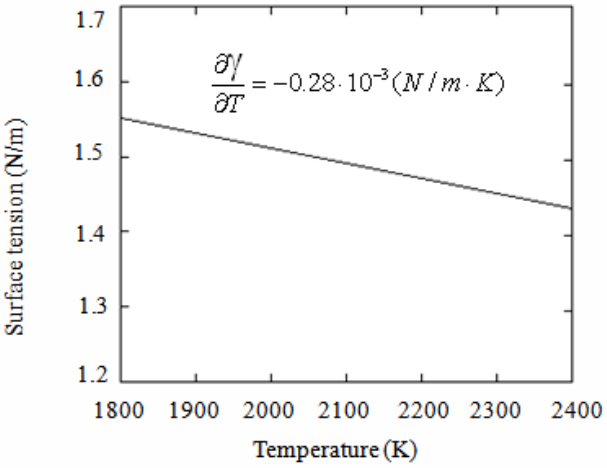

Figure 2. Surface tension of steel S235 as a function of temperature.

For experiments and simulations of the TIG welding process various geometric configurations are considered, but for all of them the following parameters were the same:

- tungsten cathode of 3.2 mm diameter,
- steel workpiece S235 of 10 mm thickness with falling surface tension characteristic,
- shielding gas is argon of the highest quality with the flow rate 12 l/min.
- time interval of simulated arc burning is 10 seconds

Figure 3 gives schematic illustration of the first pair of investigated domains with a ceramic nozzle of 11 mm diameter and two distances between electrodes: 6 mm (a) and 10 mm (b). Figure

3 (c) shows the geometry using a nozzle of 8.1 mm diameter. A welding process with tungsten cathode inside the nozzle, similar to plasma welding, was investigated with this geometry. The distance between cathode and workpiece is 16 mm.

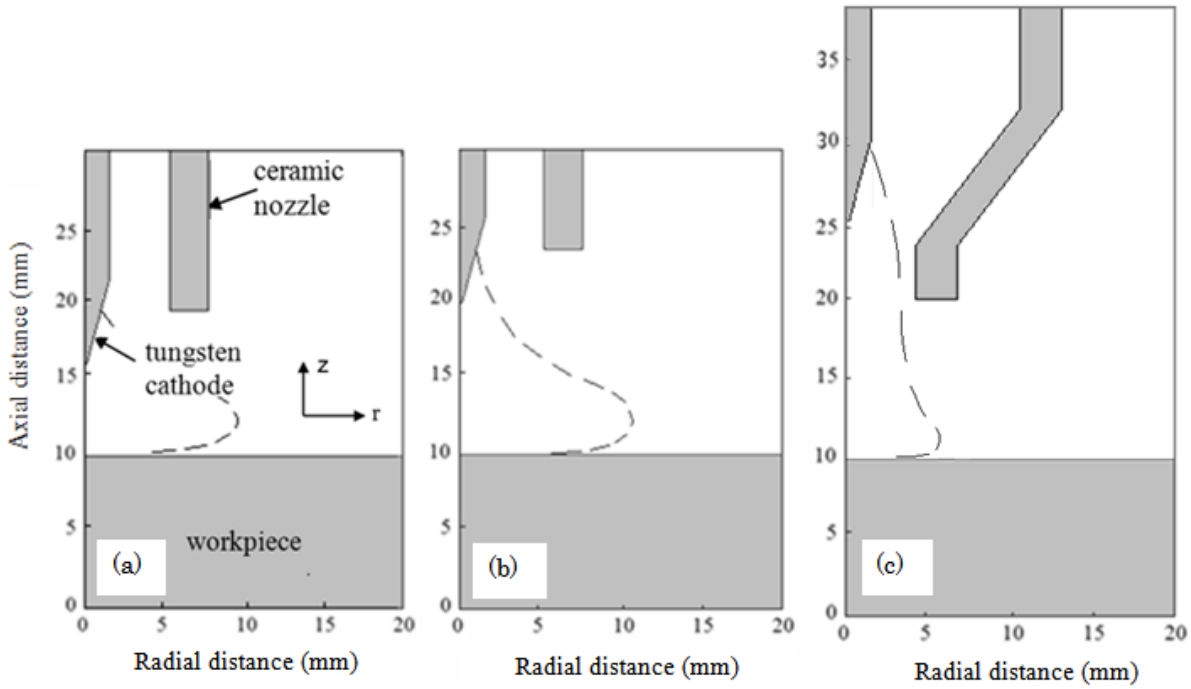

Figure 3. Investigated geometric configurations.

3. Experimental set up

For confirmation of the reliability of calculation results the following scheme of the experimental investigations has been considered: a commercial power supply is connected to the tungsten cathode surrounded by the ceramic nozzle and to the steel workpiece anode. Both, cathode and anode are fixed. The arc is ignited by the high-voltage oscillator. Argon was used as shielding inert gas with the flow rate 12 l/min. The time of anode heating is 10 seconds.

Spectroscopic measurements of plasma temperature are based on the investigations of absolute intensities of the argon spectrum line 696.54 nm [6, 7, 8] over the arc cross section at three axial positions: in the centre of the arc column, 1 mm in front of the cathode and 1 mm in front of the workpiece-anode. The arc was imaged by means of a spherical mirror on the entrance slit of 0.75 m monochromator with intensified CCD camera (PIMAX-2, Roper Scientific) providing spectral resolution 0.05 nm and spatial resolution 0.012 mm/pixel. Abel inversion algorithm has been used to reconstruct the radial distribution of the argon line emission coefficient. The radial plasma temperature profile has been calculated using equilibrium composition calculations [9] for pure argon. The experimental study also includes the analysis of cross-sections of the workpieces and high-speed video images of the arc with spatial resolution of 0.035 mm/pixel.

4. Calculation results

Calculation results for the geometric configurations presented in figure 3 (a) and (b) (ceramic nozzle of 11 mm diameter, cathode tip location outside the nozzle) are shown exemplary for the

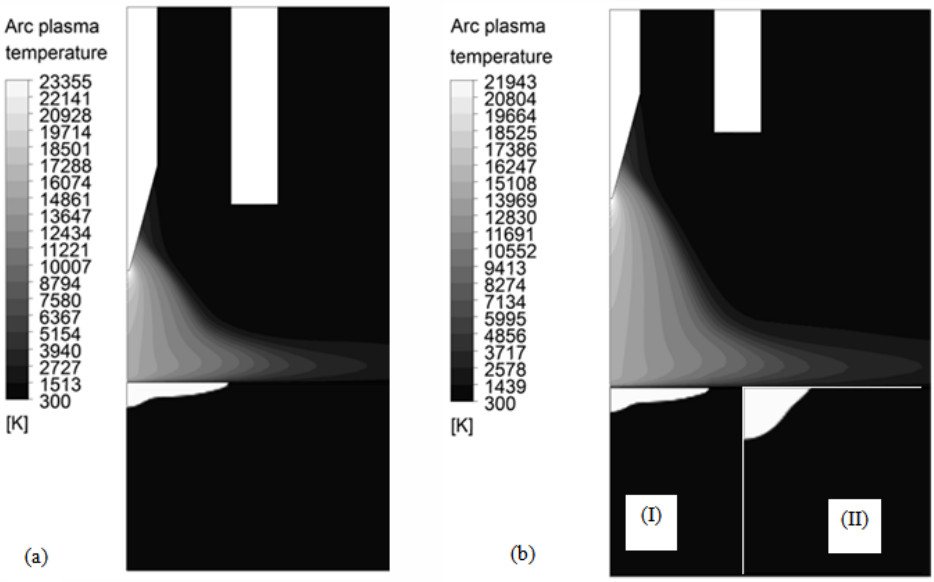

Figure 4. Weld pool profile of steel S235 and two-dimensional calculation of arc plasma temperature for an arc current of 200 A for distances between electrodes 6 mm (a) and 10 mm (b). The white area in the workpiece region indicated the molten part. In figure (b) two weld pools are calculated – with (I) and without (II) inclusion of Marangoni force.

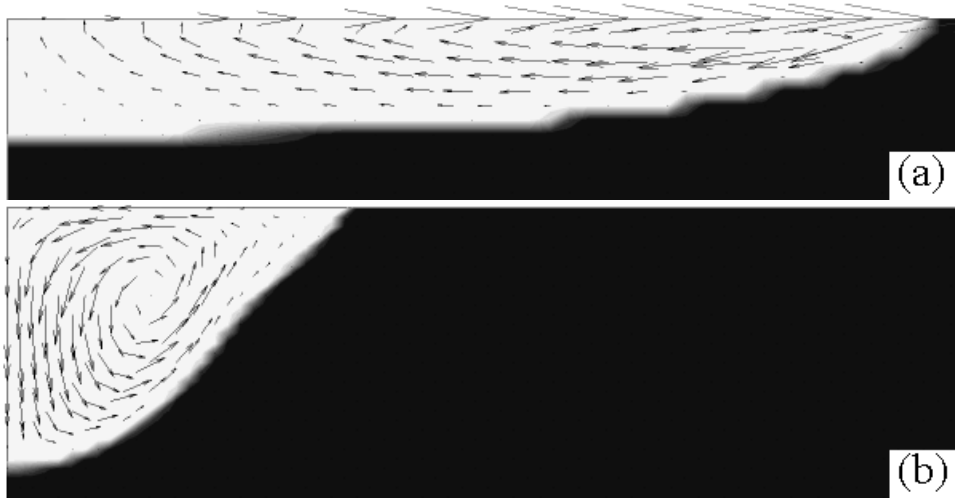

Figure 5. Flow vectors in the weld pool with (a) and without (b) inclusion of Marangoni force in the calculation model. Results are shown for mild steel S235 and current 150A.

current of 200 A in figures 4 (a) and (b), for 150 A in figure 6 (a) and for 100 A in figure 6 (b). For an arc current of 200 A and distance between electrodes 6 mm the width of weld pool is 11.5 mm, penetration depth is 1.4 mm. For the same current, but for distance 10 mm the width is 10 mm and depth is 1.4 mm. Figure 4 (b) also shows two variations of weld pool profile: I - is the weld pool calculation with Marangoni force addition and II-without it. The flow vectors diagrams for both cases are shown in figures 5(a) and (b) respectively. The observed directions of the flow correspond to those in figure 1 and confirm the data obtained in [1, 2, 3].

Decreasing the arc current to 150 A (figure 6 (a)) and to 100 A (figure 6 (b)) the width of

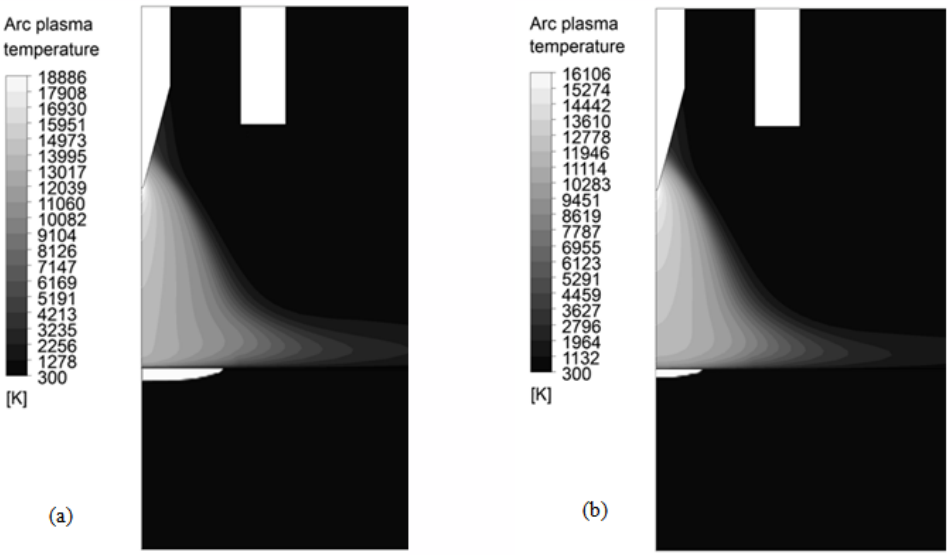

Figure 6. Weld pool profile and arc plasma temperature as in figure 4(b) for an arc current of 150 A (a) and 100 A (b) and 10 mm distance between electrodes.

the weld pool is decreased down to 8.5 mm and 5 mm, the depth down to 0.9 mm and 0.5 mm, respectively.

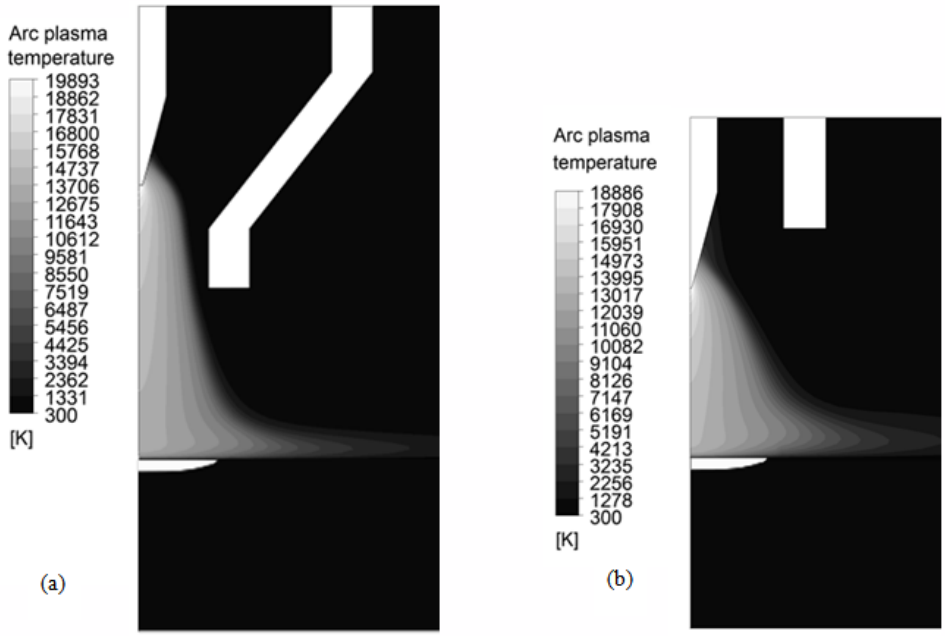

Figure 7. Weld pool profile and arc plasma temperature as in figure 4 for an arc current of 150 A for plasma arc (a) (configuration as in figure 3 (c)) and for TIG arc (b) (configuration as in figure 3 (b)).

The calculated arc temperature and weld pool profile for the geometry presented in figure 3 (c) (ceramic nozzle of 11 mm diameter, cathode tip location inside the nozzle) are shown for

an arc current of 150 A in figure 7 (a). Comparing these results with figure 6 (a) (represented also in figure 7 (b) for better visibility) shows that the plasma arc is considerably straighter and more focussed than the TIG arc. Consequently, the arc temperature is increased.

The process described in figure 7 (a) has similarities with plasma welding. However, it didnt give the expected weld pool parameters: the width of weld pool of plasma and TIG welding is the same and penetration is just a little bit deeper for plasma welding. This is due to the fact that the process was similar but not real plasma welding and the second nozzle, producing the cooling of weld pool border, wasnt used.

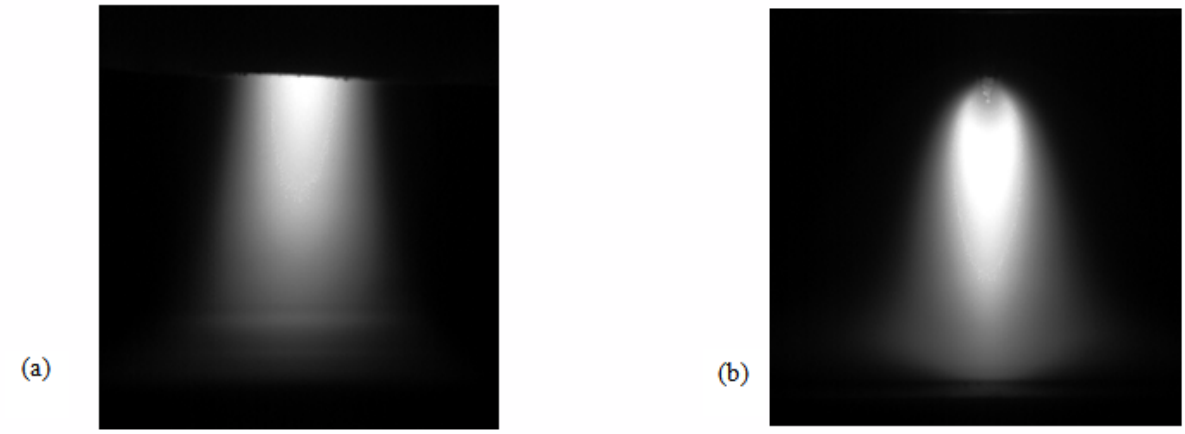

Figure 8. High speed images of the plasma arc (a) and the TIG arc (b).

The images of plasma and TIG welding arc from high-speed cameras are shown in figure 8. The general shape of the arc corresponding to the argon radiation is in good agreement with the shape of the hot regions in the calculated temperature distributions shown in figure 7.

A more detailed validation of the calculations and the model is obtained from the comparison with the results of optical emission spectroscopy for the configuration in figure 3(a) (200 A, 6 mm electrode distance). The radial distributions of plasma temperature reconstructed from the argon line radiation are shown in figure 9 as wide strip. Width of the strip corresponds to estimated experimental error. There are two main sources of experimental uncertainty. First is related to slight asymmetry of the arc which leads to certain ambiguity of the Abel transformation. Second is related to instability of the Abel inversion when emission coefficient passes normal maximum and is only relevant for temperatures above 15000 K. The lines in figure 9 correspond to the calculated two-dimensional distribution in figure 4 (a). A very good agreement has been observed within the accuracy range of the experimental results indicated in the figure.

The cross-sections of the workpieces for a TIG welding arc current of 200 A (a), 150 A (b), and 100 A (c) and distance between electrodes 10 mm are shown and compared with calculated results in figure 10. The form of the weld pool changes with rising electric current. Apart from increasing size one additional feature can be observed. The deepening in the center of the weld pool appears at 200 A. The explanation of this behaviour lies in the mutual balance of the forces which are acting on the melt. As we said before, four forces are acting on the weld pool and Marangoni force is the most important. For higher currents the efficiency of the electromagnetic force affecting the profile of the weld pool is increasing. Thus for currents higher than 200 A the deepening in the centre of weld pool appears.

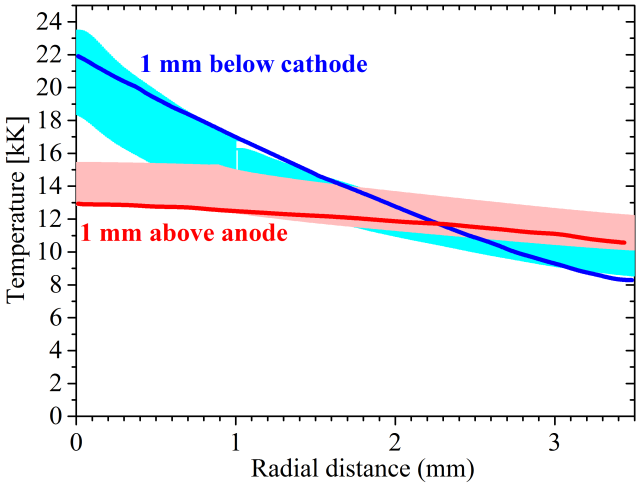

Figure 9. Comparison of TIG welding arc temperature profiles form optical emission spectroscopy (coloured strips) with calculated result (solid curves) for an arc current of 200 A and electrode distance 6 mm.

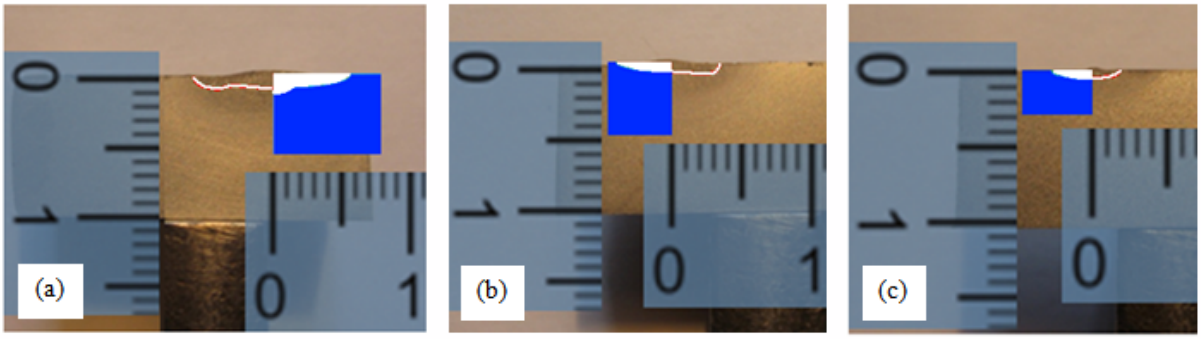

Figure 10. Cross-sections of the workpieces for a TIG welding arc current of 200 A (a), 150 A (b), 100 A (c) and electrode distance 10 mm. Comparison with calculated results.

5. Summary

Comparison of the experimental arc temperature distribution, cross-sections of the workpieces, and images from high-speed cameras shows good agreement with computational results. Herewith the computational model of a coupled magneto-hydrodynamic simulation of the welding arc and the fluid description of the weldpool has been verified succesfully. The surface tension, calculated by simple equations popular in moulding industry gave the reliable value for mild steel in a TIG welding process. The necessity of consideration of the Marangoni force in the model is shown.

Reasons of remaining insignificant differences between model and experimental results are asymmetry of the real plasma arc and neglecting of metal vapour, turbulence of plasma flow and the movement of weld pool surface in the model. For better calculation quality these effects should be considered in future work.

References

[1] Tanaka M and Lowke J J 2007 Predictions of weld pool profiles using plasma physics *J. Phys. D: Appl. Phys.* **40** R1 R23

[2] Tanaka M, Yamamoto K, Tashiro S, Nakate K, Yamamaoto E, Yamazaki K, Suzuki K, Murphy A B and

Lowke J J 2010 Time-dependent calculations of molten pool formation and thermal plasma with metal vapour in gas tungsten arc welding *J. Phys. D:Appl. Phys.* **43** 434009 (11 pp)
[3] Mougenot J, Gonzalez J-J, Freton P and Masquère M 2010 Plasmaweld pool interaction in tungsten inert-gas con-figuration *J. Phys. D:Appl. Phys.***46** 135206 (14 pp)
[4] Murphy A B and Arundell C J 1994 Transport coefficients of argon, nitrogen, oxygen, argon-nitrogen and argon-oxygen plasmas *Plasma Chem. Plasma process* **14** 451
[5] Menart J, Heberlein J V R and Pfender E 1999 Theoretical radiative transport results for a free-burning arc using a line-by-line technique *J. Phys. D:Appl. Phys.* **32** 55
[6] Olsen H N 1963 The Electric arc as a light source for quantitative spectroscopy *J. Quant. Spectrosc. Radiat. Transfer.* **3** 305-333
[7] G. N. Haddad G N and Farmer A J D 1984 Temperature determinations in a free-burning arc: 1. Experimental techniques and results in argon *J . Phys. D: Appl. Phys.* **17** 1189-1196
[8] G. Wilhelm G, Kozakov R, Goett G, Schoepp H and Uhrlandt D 2012 Behaviour of the iron vapour core in the arc of a controlled short-arc GMAW process with different shielding gases *J. Phys. D: Appl. Phys.* **45** 085202 (11pp)
[9] Wendt M 2011 Net emission coefficients of argon iron plasmas with electron Stark widths scaled to experiments *J. Phys. D: Appl. Phys.* **44** 125201
[10] Toropchin A, Frolov V and Uhrlandt D 2013 Calculation of the weld pool profile coupled with the arc simulation in a TIG process using software ANSYS CFX *Proc. XXth Symposium on Physics of Switching Arc* (Brno 2013) Editors: Aubrecht V, Bartlova M 301-304
[11] Popel S I, Sotnikov A I 1986 Theory of metallurgical processes *Metallurgy* (Moscow) 139
[12] Popel S I 1994 Surface effects in liquids *Metallurgy* (Moscow) 432